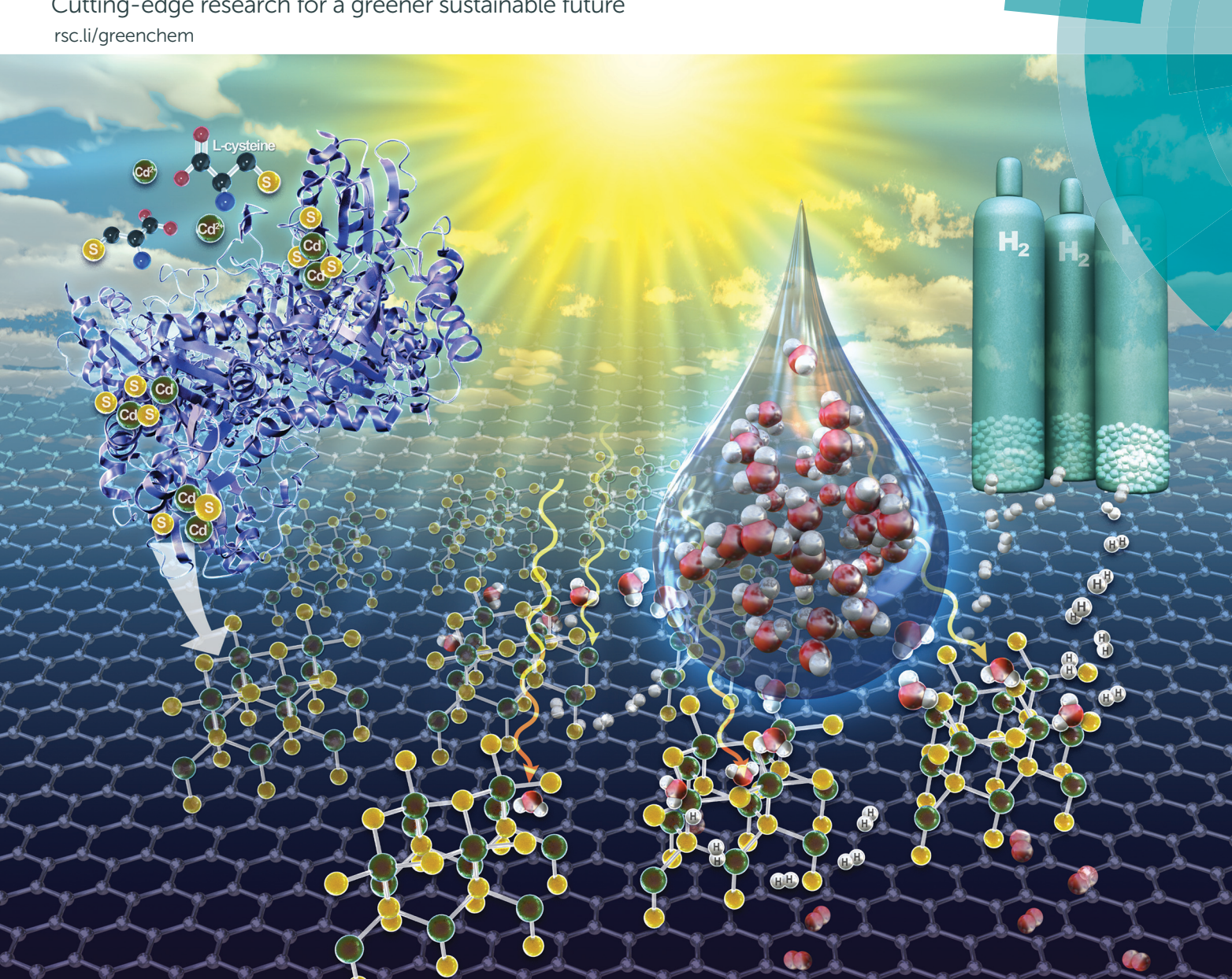
Green Chemistry

Cutting-edge research for a greener sustainable future



ISSN 1463-9262



Green Chemistry



PAPER View Article Online
View Journal | View Issue



Cite this: *Green Chem.*, 2019, **21**, 4046

Received 10th January 2019, Accepted 7th May 2019 DOI: 10.1039/c9gc00097f rsc.li/greenchem

Enzymatic synthesis of supported CdS quantum dot/reduced graphene oxide photocatalysts†

Leah C. Spangler, ^a Joseph P. Cline, ^b John D. Sakizadeh, ^a Christopher J. Kiely ^{a,b} and Steven McIntosh ^b *

Photocatalysis is an attractive, sustainable, and potentially low-cost route to capture solar energy as fuel. However, current photocatalytic materials synthesis routes are not easily scaled-up to the magnitude required to impact our energy consumption due to both economic and environmental concerns. While the elements utilized are often earth abundant, typical synthetic routes utilize organic solvents at elevated temperatures with relatively expensive precursors. Herein, we demonstrate the fully biomineralized synthesis of a quantum confined CdS/reduced graphene oxide (CdS/rGO) photocatalyst catalyzed by the single enzyme cystathionine γ -lyase (CSE). The synthesis is performed at pH 9 in a buffered aqueous solution, under ambient conditions, and utilizes the low-cost precursors Cd acetate, L-cysteine, graphene oxide, and a poly-L-lysine linker molecule. CSE actively decomposes L-cysteine to generate reactive HSin aqueous solution at pH 9. Careful selection and control of the synthesis conditions enable both reduction of graphene oxide to rGO, and control over the mean CdS nanocrystal size. The CdS is conjugated to the rGO via a poly-L-lysine crosslinker molecule introduced during rGO formation. The completed CdS/rGO photocatalyst is capable of producing H₂, without the aid of a noble metal co-catalyst, at a rate of 550 μ mol h⁻¹ q⁻¹ for an optimized CdS/rGO ratio. This rate is double that measured for unsupported CdS and is comparable to CdS/rGO photocatalysts produced using more typical chemical synthesis routes. Single enzyme biomineralization by CSE can produce a range of metal chalcogenides without altering the enzyme or benign approach, making this an easily adaptable procedure for the sustainable production of a wide variety of important photocatalyst systems.

Introduction

The global energy crisis, spurred by rapid population growth and a warming climate, has become one of the most pressing issues of the 21st century.¹ Increased worldwide energy consumption cannot be maintained using traditional energy production methods which rely on a finite source of fossil fuels. One of the most promising alternative approaches is photocatalysis, whereby solar energy is directly utilized to generate chemical fuels, such as hydrogen and light hydrocarbons, from water and carbon dioxide.² Towards this goal, heterostructured photocatalysts are particularly well suited as different materials can be coupled together to meet the demanding requirements of efficient photon capture, fast

charge separation, and catalytic activity towards the desired reaction.³ Several groups have demonstrated such photocatalysts, typically synthesized utilizing high temperature and/or pressure conditions, in the organic phase from expensive precursors.4-6 These studies inspire material design and provide critical insight into the fundamentals of photocatalytic systems; however, making an impact at the scale of global energy demand will require photocatalysts to be synthesized at an unprecedented scale. This will require low cost, low energy demand, and environmentally benign synthesis routes to facilitate a scalable green revolution. Inspired by this challenge, we report the first example of size controlled CdS nanocrystal/reduced graphene oxide (CdS/rGO) photocatalyst where both components are synthesized via single enzyme biomineralization; a low temperature, ambient pressure, aqueous phase route for sustainable material synthesis.

Biomineralization, the process by which biological systems create inorganic materials,⁷ is typically utilized to form structural materials; however, interest in the biomineralization of functional materials is growing, particularly to address materials for energy applications.^{8,9} Several groups have previously reported metal chalcogenide biomineralization in

^aDepartment of Chemical and Biomolecular Engineering, Lehigh University, Bethlehem, PA 18015, USA. E-mail: mcintosh@lehigh.edu

^bDepartment of Materials Science and Engineering, Lehigh University, Bethlehem, PA 18015 USA

[†]Electronic supplementary information (ESI) available. See DOI: 10.1039/c9gc00097f

yeasts, ^{10,11} bacteria, ^{10,12} and even higher order organisms such as earthworms. ¹³ This prior work is complemented by several groups utilizing biomolecules as templating and stabilizing molecules for bioinspired chemical synthesis of nanomaterials. ^{14–18} The challenge to overcome is engineering a biomineralization process to achieve control over the functional properties of the materials, in this case particle size and crystallinity, and produce the material in a form pure enough for the target application.

Over the past several years, our group has developed a single enzyme approach for biomineralization of size controlled, quantum confined metal sulfide nanocrystals. 19 This realizes biomineralization in perhaps it's simplest form; a single cystathionine γ-lyase enzyme (CSE), a metal precursor, and an amino acid sulfur source in a buffered solution. The removal of the need for a living organism simplifies material purification and enables the tighter control over synthesis parameters required to synthesize size-controlled nanoparticles as pure materials, alloys, and core-shell heterostructures. This high degree of control is important for their successful incorporation into quantum dot sensitized solar cells and for use as fluorescent markers in cell tagging. 20,21 Herein, we push this single-enzyme concept further to biomineralize both components of an active CdS/rGO composite photocatalyst.

CdS nanocrystals are suitable for water splitting photocatalysis due to their adequate band-gap of at least 2.4 eV, and the more negative conduction band potential of CdS compared to TiO₂.²² Supporting CdS nanocrystals on water soluble reduced graphene oxide (rGO)^{23,24} has been demonstrated by several groups to improve both the activity and stability of the photocatalyst.²⁵ Despite its favorable optical properties, the performance of unsupported CdS is limited by high exciton recombination rates and photo-corrosion effects. Supporting CdS on rGO improves photostability by preventing aggregation during the reaction²² and may provide additional sites for hydrogen generation.²⁶ Furthermore, rGO has a redox potential, ranging from -0.11 to -0.30 V depending on the degree of oxidation, below the CdS conduction band, -0.52 V,²⁷ resulting in thermodynamically favorable electron transfer from CdS to

rGO.²⁸ When combined with the high conductivity of rGO, these two factors can reduce exciton recombination rates by promoting the fast transfer of electrons away from the CdS particle.²⁶ In the present case, we report the first example of rGO biosynthesis using a single enzyme to rapidly generate low concentrations of H₂S, allowing effective reduction of graphene oxide (GO) as a green alternative to the more typically used reducing agents, namely hydrazine and sodium borohydride.

We utilize the linker molecule poly-L-lysine (PLL) to directly attach the CdS nanocrystals to the rGO surface, as has been previously demonstrated in the synthesis of fluorescent probes and cancer therapy agents. ^{29,30} PLL is similar to serine proteins with the capacity to bind to rGO, ³¹ but has the advantage that it is a much shorter peptide, which should serve to improve the transfer efficiency of photogenerated electrons into the rGO support. ³⁰ Conjugation of PLL is performed at room temperature and does not affect the properties of either rGO or CdS, making it an ideal linker molecule for the biomineralized CdS/rGO photocatalyst.

Results and discussion

Enzymatic reduction of GO

Incubation of GO in a buffered aqueous solution containing L-cysteine amino acid and CSE results in a color change from brown to black, indicative of GO reduction to rGO, in as little as 2 h. This rapid reduction occurs through the CSE catalyzed enzymatic decomposition of L-cysteine to form reactive sulfur species in solution.³² We utilize the same aqueous, ambient temperature, reaction sequence herein, and described in detail in prior publications, to enable biomineralization of metal sulfide QDs,^{19–21,33–35} Fig. 1 provides evidence for this GO reduction process *via* the UV-vis, FTIR and Raman spectra of as-synthesized GO, and the same GO material incubated for 4 h either with L-cysteine or with a mixture of L-cysteine and CSE. All samples were suspended in Tris buffer and, besides the as-synthesized GO, contain PLL as a linker molecule for subsequent functionalization with CdS QDs.

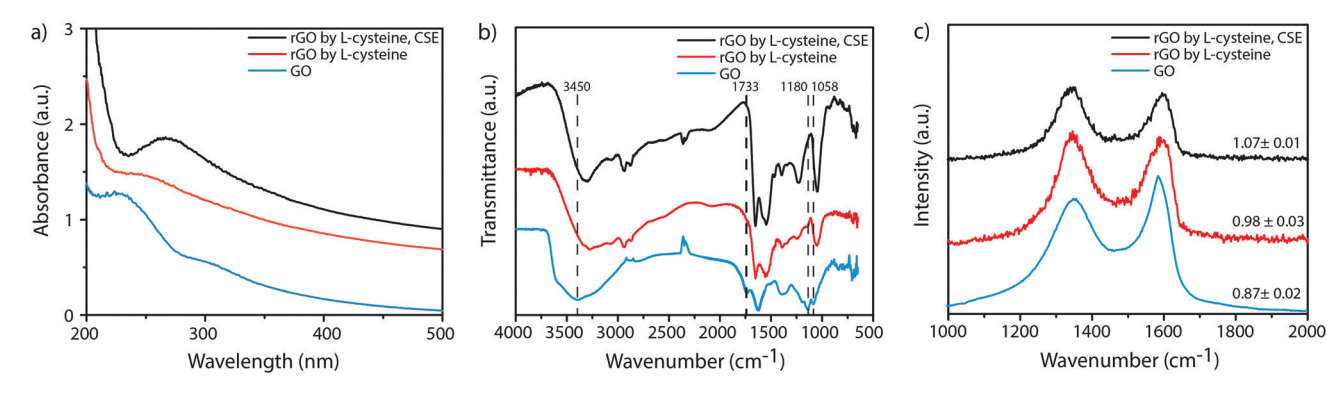


Fig. 1 (a) UV-vis absorbance, (b) FTIR and (c) Raman spectra of: 0.2 g L $^{-1}$ GO synthesized using the modified Hummers' method; the same GO incubated with 10 mM $_{\rm L}$ -cysteine and 0.05 mg mL $^{-1}$ CSE enzyme for 4 h. The latter two samples also contain 0.8 mg mL $^{-1}$ PLL.

Paper

The UV-vis spectrum of the as-synthesized GO, (Fig. 1a), shows the expected absorbance peak at 230 nm and shoulder at 300 nm, attributed to energy adsorption by aromatic C-C bonds within the GO sheets and by C=O bonds on the GO surface, respectively.³⁶ Incubation with L-cysteine and CSE leads to an absorbance peak shift from 230 to 270 nm and the simultaneous disappearance of the shoulder at 300 nm. These changes are attributable to the restoration of sp² hybridization of the C-C bonds in the product rGO sheet, and the reduction of the surface C=O bonds, respectively, providing evidence for the enzymatic reduction process.³⁷ In contrast, attempts to reduce GO by L-cysteine alone in the absence of CSE results in a less definitive reduction without a clear shift in the absorption peak position. Instead, the primary absorption peak becomes poorly defined. This agrees with previous reports of slow GO reduction by high concentrations of L-cysteine alone, which takes over 72 h at room temperature due to the weak reducing power of L-cysteine. 38 Reduction can be accelerated at temperatures and pressures high enough to thermally decompose L-cysteine, 39 although this of course loses the ambient temperature synthesis target of our work. Note that no reduction is observed in the absence of L-cysteine, even with the enzyme present (Fig. S1†). Hence CSE is critical in catalyzing the efficient reduction of GO by L-cysteine. This deduction is further supported by complementary FTIR (Fig. 1b), and Raman spectroscopy (Fig. 1c) evidence.

The characteristic FTIR peaks of GO are located at 3450 cm⁻¹ (O-H stretching), 1733 cm⁻¹ (C=O stretching), 1180 cm⁻¹ (C-O), and 1058 cm⁻¹ (C-O stretching).⁴⁰ The peaks at 1733, 1180, and 1058 cm⁻¹ are completely eliminated following CSE catalyzed reduction of GO, corresponding to C-O and C=O bond elimination. The absence of all carbon-oxygen bonds means that any oxygen groups on the surface of the GO sheet have been removed, forming the final rGO material (Fig. 1b). These same peak intensities are also substantially decreased following reduction by L-cysteine in the absence of CSE. However, shoulder peaks still exist in the spectra at these characteristic positions (Fig. 1b) indicating some C=O and C-O bonds remain and thus less reduction is achieved. The large FTIR peak at 3450 cm⁻¹ corresponds to the presence of hydroxyl species either as -OH groups on the carbon surface, or from water intercalated between the dried sheets. 41 This peak appears to shift significantly to 3270 cm⁻¹ following reduction using L-cysteine, both with and without CSE. However, this shift is not caused by reduction, but instead by the introduction of the PLL ligand on the surface of the rGO samples. 42 The presence of PLL complicates the analysis of the 3450 cm⁻¹ signal. However, the peak appears to be reduced when compared to the original GO sample, agreeing with the disappearance of the other C-O bonds. The GO spectrum also shows a small peak at 1620 cm⁻¹ corresponding to C-C bonding in the graphene sheets. 40 Again, this peak is obscured by the PLL ligand peaks in the other two rGO spectra. 42

The degree of this enzymatic reduction can be semi-quantified by comparing the relative intensities of the disordered carbon D band (1340 cm $^{-1}$) and graphitic E_{2g} G band

(1580 cm $^{-1}$) peaks in Raman spectra (Fig. 1c). 43,44 The D/G intensity ratio increases from 0.87 \pm 0.02 for GO, to 0.98 \pm 0.03 for GO reduced by L-cysteine alone, and to 1.07 \pm 0.01 for GO reduced by L-cysteine and catalyzed by CSE (Fig. 1c). As discussed by Stankovich *et al.* an increase in the D/G band ratio upon reduction of GO is indicative of an increased number of smaller sized sp 2 hybridized domains in the reduced material. 24 This ratio is typically utilized as an indication of the extent of reduction of the material, which further supports our proposition, demonstrated by UV-vis and FTIR spectroscopies, that CSE acts to catalyze GO reduction in the presence of L-cysteine.

This enzymatic reduction process most likely occurs through the active turnover of L-cysteine by CSE to form H₂S in solution. ^{34,45} At pH 9, H₂S dissociates to HS⁻ which acts as a strong reducing agent on C–O and C=O species under basic conditions. ^{32,46} H₂S is not commonly utilized as a reductant in the laboratory due to the potential toxicity when supplied and stored in a concentrated form. ³⁹ In contrast, our controlled, point of use, enzymatic generation of dilute H₂S from benign precursors enables tight control over the biomineralization and reduction process. ³⁴ Thus, while L-cysteine is only a weak and slow reducing agent in its own, we enable the use of this benign sulfur source *via* the biomineralization inspired use of the CSE enzyme to decompose L-cysteine and generate H₂S as a strong reducing agent to yield an increased extent of GO reduction over the same time period.

Several groups have previously reported other ambient, bioinspired, methods for the partial reduction of GO, including amino acids, ^{38,47} phytoextracts, ⁴⁸ and metal reducing organisms. ^{49–51} Dissimilatory metal reducing bacteria, such as the *Sewanella* species, have also been demonstrated to reduce GO using pre-existing extracellular electron transfer pathways. ⁵⁰ However, scale-up of these processes is not economically viable as the cells need to be grown and maintained, as well as separated from the product following synthesis. ⁵² For a cleaner process, proteins such as bovine serum albumin (BSA) have been shown to reduce GO; however, elevated temperatures (55–90 °C) are still required. Our proposed GO reduction method does not suffer from these disadvantages and so is inherently capable of being scaled-up in an economic fashion.

Biomineralization of quantum confined CdS nanocrystals and their subsequent attachment to rGO

Conveniently, the cystathionine γ -lyase (CSE) enzyme and mechanism by which it operates are those that we have previously engineered to achieve size controlled biomineralization of a range of quantum confined nanocrystals and heterostructures. Herein, we again utilize this established process to biomineralize quantum confined CdS nanocrystals from a buffered solution of Cd acetate and L-cysteine utilizing the same CSE as used for the GO reduction process described above. The absorbance and photoluminescence properties of these biomineralized CdS nanocrystals are shown in Fig. 2a and are consistent with our previous reports. Using the relation developed by Yu *et al.*, the absorbance peak at 390 nm

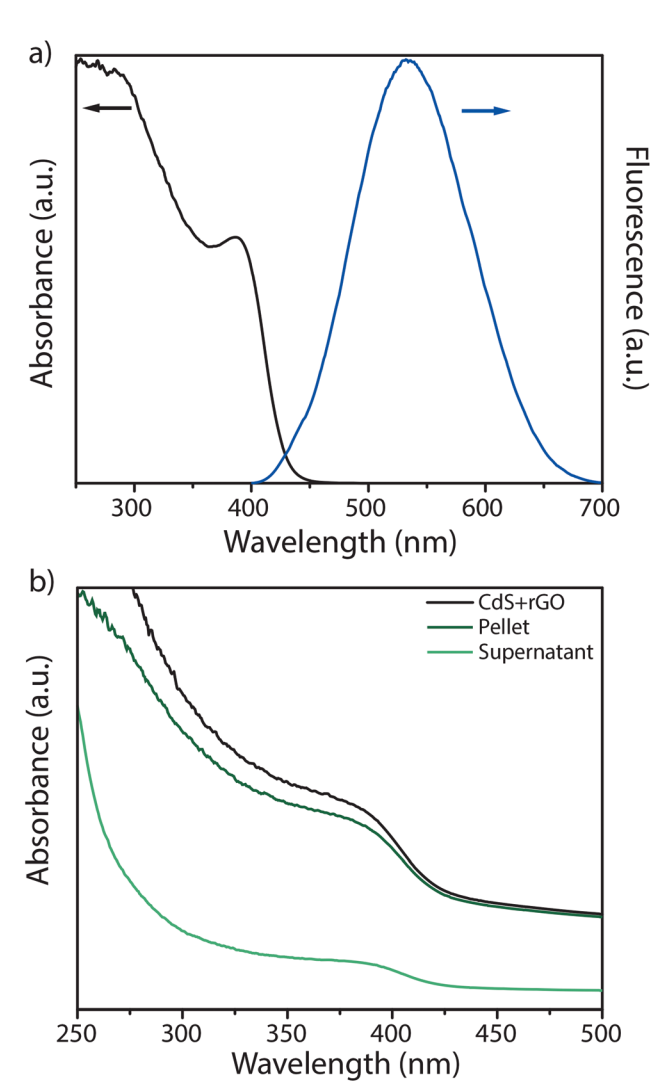


Fig. 2 (a) Typical absorbance and photoluminescence spectra of biomineralized CdS nanocrystals. (b) Absorbance spectra of (i) the CdS/rGO mixture prior to centrifugation, (ii) the re-suspended pellet containing CdS/rGO and (iii) the separated supernatant containing unattached CdS.

can be used to estimate the diameter of the CdS nanocrystals as approximately 3.0 nm. 53 This value agrees with our previous study utilizing the same process where absorption peaks of 330 nm and 350 nm corresponded respectively to particle diameters of 2.06 \pm 0.45 nm and 2.44 \pm 0.46 nm as determined by HAADF-STEM analysis. 34 Thus we can utilize the same engineered biomineralization process to produce both of the primary components of the photocatalyst, namely the rGO and CdS, in aqueous media at ambient temperature and pressure from abundant and benign precursors.

These two components can then be conjugated in the aqueous phase *via* poly-L-lysine (PLL) linker.²⁹ In this case PLL was attached to the rGO surface during the reduction process. Fig. 2b shows the absorbance spectra of (i) a solution containing the CdS nanocrystals and PLL functionalized rGO prior to centrifugation, (ii) the supernatant following centrifugation, and (iii) the thoroughly washed centrifugation pellet re-sus-

pended in DI water. Prior to centrifugation, a strong CdS nanocrystal absorbance peak starting at 390 nm is clearly visible above the high and broad rGO absorption background. The resuspended centrifuged pellet retains both this nanocrystal absorbance peak and rGO background. In contrast, the supernatant spectrum shows a small residual peak at 390 nm indicating only a small residue of unattached CdS nanocrystals. Control experiments confirmed that the small as-synthesized, unattached QDs cannot be separated by centrifugation under these conditions, but that the rGO can be centrifuged from solution. The co-existence of the CdS nanocrystal absorption peak with the rGO background in the resuspended pellet demonstrates conjugation of the CdS to rGO to form a fully biomineralized CdS/rGO composite photocatalyst. The entire synthesis process to generate our CdS/rGO heterostructured photocatalyst is illustrated in Fig. 3. Biomineralization of both rGO and CdS components as well as their subsequent attachment using PLL are shown.

Definitive confirmation of CdS QD attachment to rGO is provided by electron microscopy imaging. Fig. 4a is a brightfield scanning transmission electron microscopy (BF-STEM) image of the CdS/rGO photocatalyst supported on a holey carbon film. Note that no unassociated QDs were found on the holey carbon film indicating the QDs were strongly bound to the rGO sheets prior to drying the sample onto the grid. A higher magnification high angle annular dark field (HAADF-STEM) image, Fig. 4b, confirms the crystallinity of the particles. The two possible CdS crystal polymorphs are the hexagonal wurtzite and face centered cubic (fcc) zinc blende type structures. Fig. 4c and d show atomic resolution HAADF-STEM images of CdS particles on rGO with d-spacings and angles that are consistent with both crystal structures (see Fig. S2, Tables S1 and S2†). Fig. 4e and f show individual CdS particles on rGO along directions that can be definitively associated with the [101] projection of the wurtzite and [001] projection of the zinc blende structures of CdS, respectively (see Fig. S3 and Table S3†). Hence, we have clear evidence that both CdS polymorphs are produced by the enzymatic biomineralization process and that both persist when the particles are immobilized on the rGO support. The presence of both polymorphs is consistent with prior reports of CdS biomineralized nanocrystals.33

Hydrogen production of the fully biomineralized CdS/rGO heterostructured photocatalysts

The photocatalytic activity of these biomineralized catalysts towards water splitting is shown in Fig. 5a, showing cumulative H₂ generated *versus* xenon lamp irradiation time for (i) the CdS/rGO composite photocatalyst, (ii) colloidal CdS nanocrystals only, and (iii) suspended rGO only. The H₂ generation rate for the CdS/rGO catalyst is pseudo first order, consistent with the expected performance of a stable photocatalyst, ⁵⁴ and shows significantly improved hydrogen generation compared to the CdS nanocrystals alone. This increased activity is attributable to increased exciton separation, due to electron donation from the CdS particles onto the rGO support. ²⁶

Paper

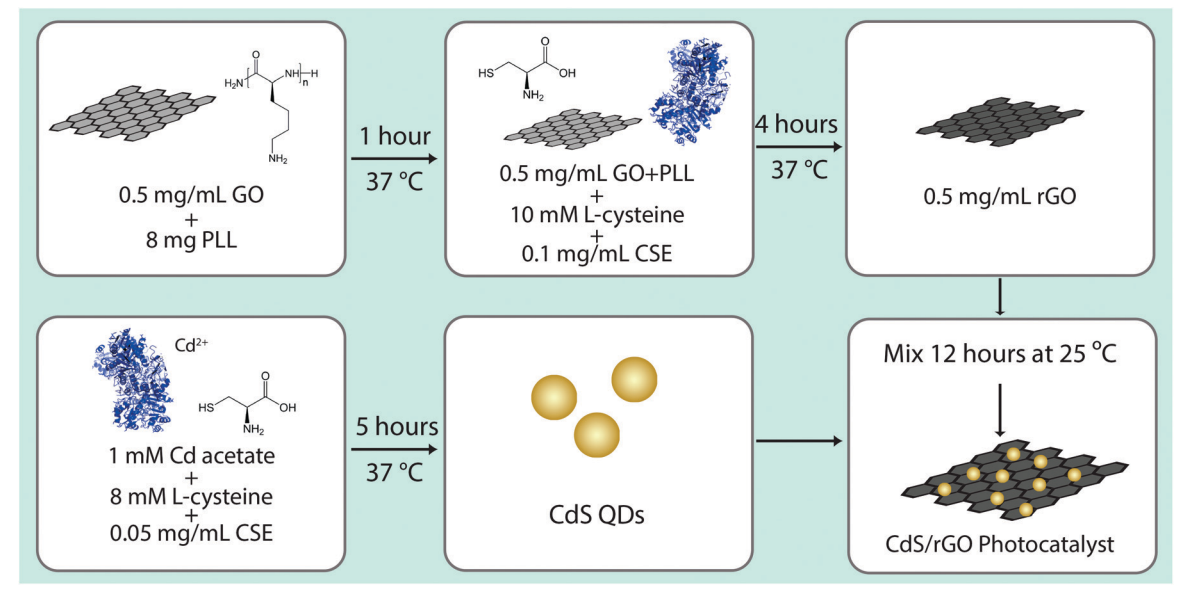


Fig. 3 A step by step illustration of the fully biomineralized synthesis used to produce the CdS/rGO photocatalyst.

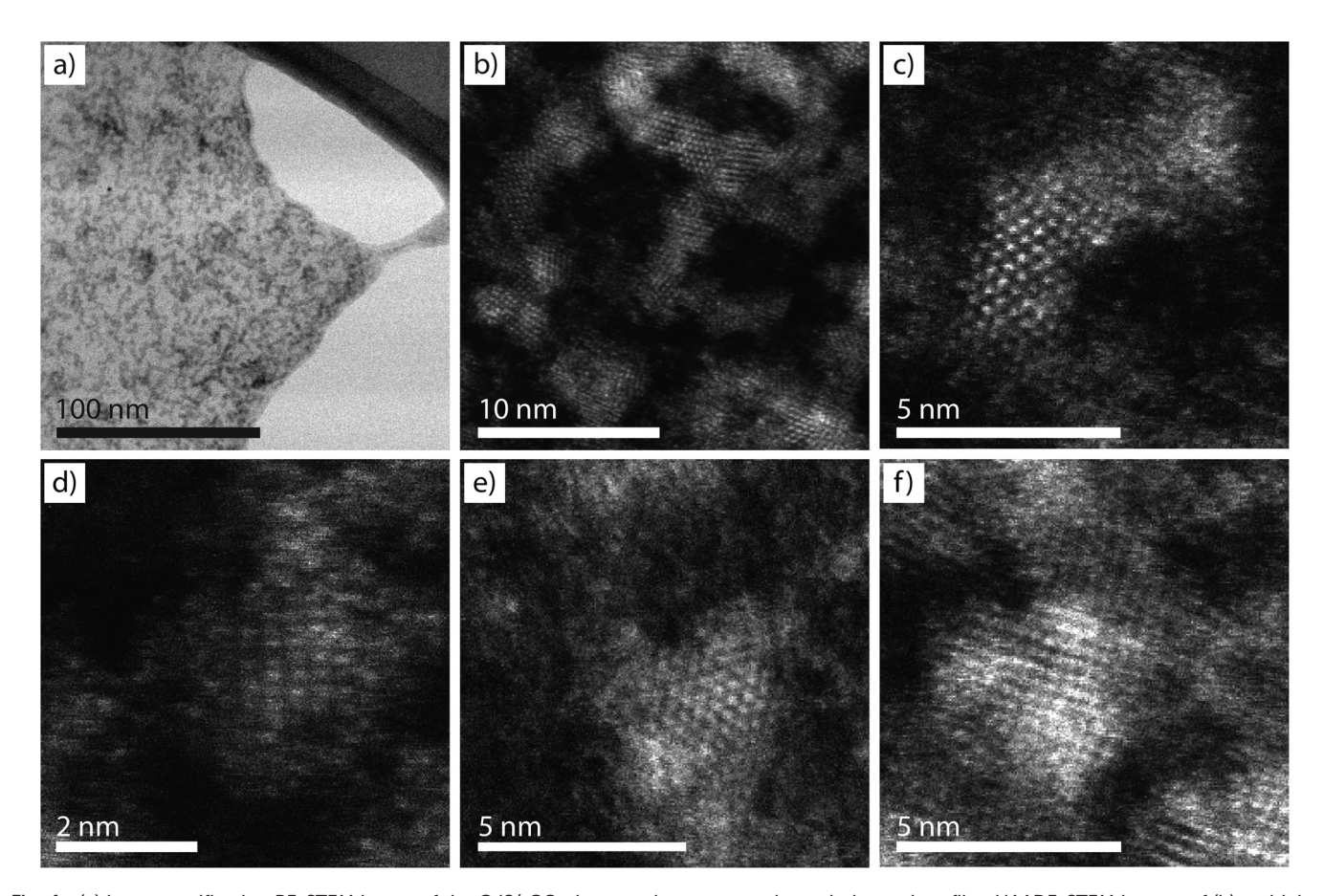
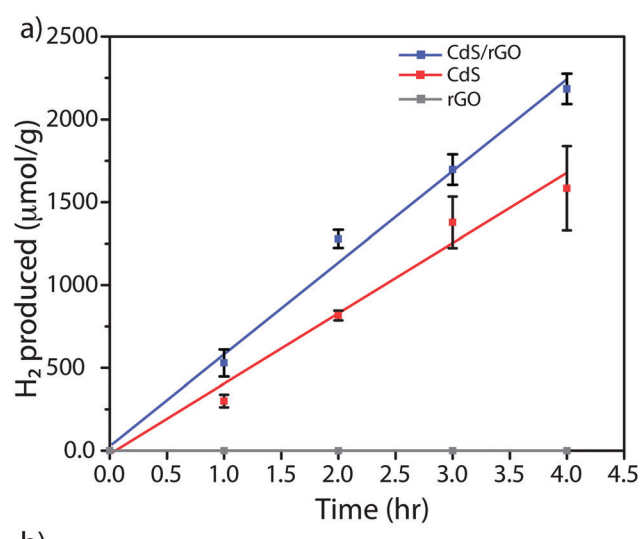


Fig. 4 (a) Low magnification BF-STEM image of the CdS/rGO photocatalyst supported on a holey carbon film. HAADF-STEM images of (b) multiple supported CdS nanocrystals; (c) a CdS nanocrystal orientation that is consistent with either the [101] wurtzite projection or [011] zinc blende projection; (d) a CdS nanocrystal orientation that is consistent with either the [210] wurtzite projection or [211] zinc blende projection; (e) a CdS particle with the wurtzite-type structure viewed along the [101] direction and (f) a CdS particle with the zinc blende structure viewed along the [001] direction.



Green Chemistry

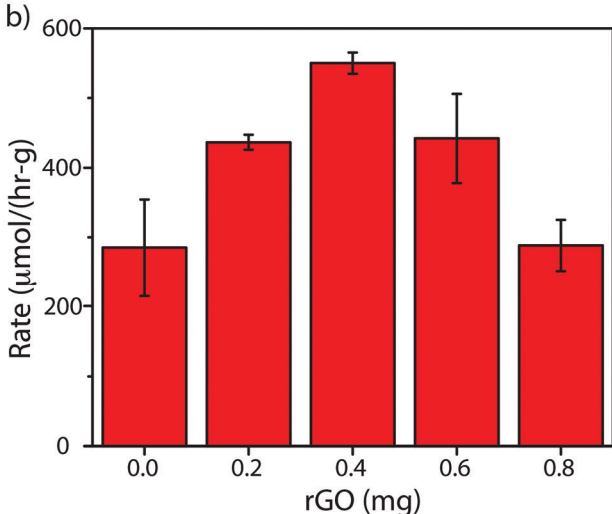


Fig. 5 (a) Hydrogen production versus reaction time data for (i) CdS/ rGO, (ii) CdS only, and (iii) rGO only. Hydrogen production was normalized by total catalyst weight for comparative purposes. (b) Hydrogen generation rate of CdS/rGO catalysts versus bare CdS, showing optimum $\rm H_2$ generation when the amount of rGO in the photoreactor was 0.4 mg.

Evidence of electron transfer from CdS to rGO was observed using TCSPC measurements (Fig. S4 and Table S3†). The unattached CdS have two lifetimes of 2.5 and 65 ns, corresponding to non-radiative and radiative pathways, respectively. When the CdS nanocrystals are attached to rGO, the non-radiative lifetime is reduced to 0.22 ns. The radiative lifetime remains the same, but the prefactor, A2, in the biexponential decay equation (shown above Table S3†) is reduced from 0.70 in the unattached nanocrystals to 0.06 in the CdS/rGO heterostructured system. The prefactor corresponds to the number of photons collected with this radiative lifetime, and shows that the amount of electrons taking this pathway is almost completely eliminated. This behavior is consistent with other studies of CdS nanocrystals on rGO and is attributed to improved charge injection of electrons from CdS into rGO. 55,56 This sup-

pression of radiative recombination is due to the charge separation occurring as the excited electron is transferred from the CdS to rGO, thus decreasing radiative exciton recombination. Increased H2 production could also result from an increased dispersion and stability of the CdS component of the photocatalyst facilitated by the rGO support. While we observed no change in the CdS/rGO catalyst during the experiment, a vellow precipitate formed at the bottom of the reactor when utilizing the unsupported CdS catalyst. This was accompanied by a decrease in the intensity of the CdS UV-vis absorption peak (Fig. S5†). The formation of the CdS precipitate is also reflected in a decrease in the amount of hydrogen produced per hour. The decline in hydrogen caused by CdS aggregation is more obvious over longer times than in the time scale shown in Fig. 5a. As shown in Fig. S6,† the hydrogen generation verses time for the CdS sample shows a decline after two hours. In contrast, the hydrogen produced verses time by the CdS/rGO composite material is consistent. Both of these effects are indicative of the commonly observed agglomeration of unsupported CdS photocatalysts.⁵⁷ It should also be noted that rGO was not capable of generating hydrogen without the addition of CdS.

The loading of CdS onto rGO was optimized with respect to hydrogen generation rate by varying the amount of rGO sensitized by CdS (Fig. 5b). A maximum in activity is observed reflecting the competing factors of increasing nanocrystal population/dispersion and decreasing light penetration as the rGO content of the solution increases, again an effect typically observed in these systems. 26,58 The highest photocatalytic activity of our CdS/rGO photocatalyst was 550 mmol h⁻¹ g⁻¹. To quantitatively show the improvement in hydrogen production from rGO, we subtracted the average H2 production rate of CdS alone from the rate for the optimized CdS/rGO composite. The difference, 265 mmol $h^{-1} g^{-1}$, is approximately equal to the H₂ generation rate of 285 mmol h⁻¹ g⁻¹ from CdS alone. Thus, the addition of rGO essentially doubles the catalytic rate. Our optimized photocatalyst rate is comparable to other reported values for similar composites with no metal cocatalyst. For example, Zhang et al. reported their highest H2 conversion rate of 1824 mmol h⁻¹ g⁻¹ for a ZnCdS/rGO nanocomposite, while Jia et al. reported a highest H2 rate of 1050 mmol h⁻¹ g⁻¹ for a CdS/rGO nanocomposite.^{58,59} One possible explanation for the higher values obtained by these groups is the use of a heating step in the preparation of CdS. For example, Zhang et al. prepared their photocatalysts by heating in an autoclave to 160 °C for 4 h. Given that our fully biomineralization approach is performed completely at room temperature, our rates are still competitive with photocatalysts prepared using routes involving higher temperature and pressure.

These results demonstrate a fully biomineralized process to synthesize CdS/rGO photocatalysts in the aqueous phase, at low temperatures and ambient pressure, from benign precursors. The resulting CdS/rGO photocatalyst can generate H₂ at rates comparable to the same composite systems produced using higher temperature routes. Indeed, we anticipate that

Paper Green Chemistry

increased catalytic activity may be achieved in our biomineralized photocatalysts through further optimization. This work demonstrates the utility of biomineralization to realize benign synthesis of functional materials for energy applications. Future work will focus on further developing and leveraging enzymatic biomineralization to incorporate advances made in understanding chemically synthesized photocatalysts, including replacing CdS with a less toxic material and the incorporation of biomineralized co-catalysts.

Conclusions

Our work demonstrates the first use of a single enzyme for the biomineralization of both CdS nanocrystals and reduced graphene oxide (rGO), and their combination to form an active photocatalyst for H₂ generation. The entire aqueous synthesis process is performed at room temperature under ambient conditions, resulting in a potentially sustainable, scalable, and lower cost process. Synthesis occurs via enzymatic turnover of L-cysteine by CSE to form H2S which then dissociates to form HS in aqueous solution at pH 9. Reduction of GO occurs in as little as 4 h due to the strong reducing power of the HSspecies. CdS nanocrystals are formed through the reaction of Cd acetate and HS⁻ in solution, with size control achieved by maintaining growth in the size focusing regime. The nanocrystals are stabilized by excess L-cysteine ligands in solution. The as-synthesized quantum confined CdS nanocrystals are conjugated to rGO utilizing a poly-1-lysine (PLL) crosslinker molecule via a simple low temperature incubation method. Optimization of the CdS/rGO ratio yields a photocatalyst that can provide H₂ generation rates from water splitting that are comparable to those of CdS/rGO photocatalysts prepared using more typical chemical approaches. The CdS nanoparticles immobilized on rGO also performed better than unsupported biomineralized CdS quantum dots alone, due to improved exciton separation and better nanocrystal stability. These promising results demonstrate the feasibility of biomineralization as a potentially sustainable and scalable approach to photocatalyst synthesis.

Experimental methods

Graphene oxide synthesis

Graphene oxide was synthesized using the modified Hummer's method.²³ A 20 g batch of graphite powder (Carbon Bay) was first oxidized by mixing with a solution of 30 mL sulfuric acid (BDH, 96%), 10 g potassium peroxisulfate (Alfa Aesar, 99%), and 10 g phosphorous pentoxide (Alfa Aesar, 99.99%) pre-heated to 80 °C. The solution was then slowly cooled to room temperature over a period of 6 h. The resulting material was diluted, filtered and washed with DI water until the rinse water reached a neutral pH. Oxidation was performed by adding the rinsed powder to a 460 mL solution of sulfuric acid cooled to 4 °C. Then 60 g of potassium permanganate

(Alfa Aesar, 99.0%) was slowly added keeping the temperature of the solution below 25 °C. The solution was subsequently heated to 35 °C for 2 h before dilution with DI water. After an additional 15 min, the reaction was stopped by further addition of DI water and 50 mL of hydrogen peroxide (BDH, 30%). The resulting graphene oxide was filtered and washed with 10% hydrogen chloride solution (BDH, 37.6%) before being re-suspended to a final concentration of 2 g L⁻¹. The GO was further purified by dialysis (Snakeskin, MWCO 3500 kDa) and several iterations of centrifuge washing to completely remove any remaining acid.

Functionalization of GO by poly-L-lysine and reduction via CSE

Enzymatic reduction of graphene oxide utilizing an L-cysteine substrate in the presence of the linker molecule poly-L-lysine (PLL, MW 30 000-50 000, Alfa Aesar)²⁹ forms a functionalized reduced graphene oxide material, rGO_{PLL}, suitable for supporting the CdS nanocrystals. To achieve this, 0.5 g L⁻¹ of purified GO was first sonicated on ice for 15 min. Following this, 8 mg of PLL was added to 10 mL of a dilute GO suspension (0.2 g L^{-1}) in 0.1 M Tris buffer (pH 9, VWR, 99.5%) and heated at 37 °C for 1 h. A small amount of precipitate was removed via centrifugation. Next, either 10 mM L-cysteine or 10 mM L-cysteine and 0.4 mg mL⁻¹ CSE were added to the GO-PLL solution and incubated for up to 4 h. The resulting rGO_{PLL} suspension was purified by several rounds of centrifuging and re-suspension in DI water in order to remove any excess PLL from solution.

Biomineralization of CdS quantum dots

Quantum confined CdS nanocrystals were synthesized by the single enzyme cystathionine γ-lyase (CSE) as previously reported. 19 CSE was overexpressed using recombinant E. coli and purified using ionic metal affinity chromatography (IMAC). Quantum dot synthesis was initiated by combining 1 mM Cd acetate (Alfa Aesar, 99.999% Puratronic), 8 mM L-cysteine, and 0.05 mg mL⁻¹ CSE in 0.1 M Tris-HCl (pH 9). The solutions were incubated at 37 °C for 5 h until a UV-vis absorbance peak at 390 nm was obtained, indicating a mean particle size of ~3.0 nm.

Preparation and testing of CdS-rGO_{PLL} photocatalysts

Conjugation of CdS quantum dot nanocrystals (QDs) and rGO_{PLL} was achieved by physically mixing the components and leaving them to incubate overnight at room temperature. After this overnight dwell, any unattached CdS QDS were separated from the rGO-CdS conjugates by centrifugation. The supernatant containing the unattached QDs was discarded, and the rGO-CdS pellet was washed twice with DI water and sonicated for 15 min before resuspension in 0.1 M Na₂S/0.1 M Na₂SO₃ to a final volume of 80 mL. Prior to initiating the water splitting photoreaction, the as-prepared photocatalyst was degassed under vacuum for 1 h in a 100 mL round bottom flask while stirring vigorously. Following the degas step, the remaining head space was purged with N2 for 15 min to ensure no oxygen was present within the reactor. The reactor was then sealed

and positioned 20 mm away from a 350 W Xenon lamp fitted with a \geq 420 nm UV cut-off filter. A 0.4 mL gas sample was obtained every hour through a septum and analyzed for hydrogen and oxygen content by a model 8610C gas chromatograph (SRI Instruments) equipped with thermal conductivity detector.

Materials characterization

Absorbance measurements were collected using a UV-vis 2600 spectrophotometer equipped with an ISR-2600-Plus integrating sphere attachment (Shimadzu). FTIR spectra were acquired using a Thermo Nicolet iS50 infrared spectrometer equipped with a mercury-cadmium-telluride (MCT) liquid nitrogen cooled detector with a Harrick Praying Mantis diffuse reflection accessory and ZnSe windows. All spectra were averaged over 96 scans at a resolution of 4 cm⁻¹. Raman spectra were obtained using an Alpha300RA confocal Raman microscope equipped with a 532 nm laser and UHTS 400NIR spectrometer with a diffraction grating of 2400 lines per mm (Witec). Photoluminescence experiments were performed using a QuantaMasterTM 400 (Photon Technology International). Photoluminescence lifetime measurements were obtained using the Fluorolog-3 spectrofluorometer with attached Time-Correlated Single Photon Counting (TCSPC) controller. The excitation source was a 287 nm laser (Delta Diode). The photoluminescence lifetimes were calculated from the decay curves using a bi-exponential fit. Samples used for scanning transmission electron microscopy (STEM) analysis were diluted ten times in DI water and dispersed as a single drop onto a holey carbon coated Cu mesh grid. The liquid content of the sample was then allowed to evaporate under vacuum overnight. The CdS/rGO_{PLL} samples were examined in bright field (BF) and high angle annular dark field (HAADF) STEM imaging modes using an aberration corrected JEOL ARM 200CF analytical electron microscope operating at 80 kV.

Conflicts of interest

There are no conflicts to declare.

Acknowledgements

This material is based upon work supported by the National Science Foundation under the EFRI-PSBR program, Grant No. 1332349 and under the SNM-IS program, Grant No. 1727166. We thank Dr Jonas Baltrusaitis of the Department of Chemical Engineering for use of the FTIR and Raman instruments. We would also like the thank Dr William Taifan of the Baltrusaitis lab for assisting with the FTIR measurements. We thank Dr Angela Brown of the Department of Chemical Engineering for use of the fluorometer. We thank Dr Damien Thevenin of the Department of Chemistry for use of the fluorometer with TCSPC controller.

References

- 1 N. S. Lewis and D. G. Nocera, *Proc. Natl. Acad. Sci. U. S. A.*, 2006, **103**, 15729–15735.
- 2 E. V. Kondratenko, G. Mul, J. Baltrusaitis, G. O. Larrazábal and J. Pérez-Ramírez, *Energy Environ. Sci.*, 2013, **6**, 3112–3135.
- 3 H. Zhou, Y. Qu, T. Zeid and X. Duan, *Energy Environ. Sci.*, 2012, 5, 6732–6743.
- 4 C. B. Murray, D. J. Norris and M. G. Bawendi, J. Am. Chem. Soc., 1993, 115, 8706–8715.
- 5 Y. Qu and X. Duan, Chem. Soc. Rev., 2013, 42, 2568-2580.
- 6 Y. Wang, Q. Wang, X. Zhan, F. Wang, M. Safdar and J. He, *Nanoscale*, 2013, 5, 8326–8339.
- 7 S. Mann, Biomineralization: principles and concepts in bioinorganic materials chemistry, Oxford University Press, 2001, vol. 5.
- 8 F. Nudelman and N. A. Sommerdijk, *Angew. Chem., Int. Ed.*, 2012, **51**, 6582–6596.
- 9 A. Arakaki, K. Shimizu, M. Oda, T. Sakamoto, T. Nishimura and T. Kato, *Org. Biomol. Chem.*, 2015, **13**, 974–989.
- 10 C. Dameron, R. Reese, R. Mehra, A. Kortan, P. Carroll, M. Steigerwald, L. Brus and D. Winge, *Nature*, 1989, 338, 596–597.
- 11 T. Yano, H. Fukamachi, M. Yamamoto and T. Igarashi, *Oral Microbiol. Immunol.*, 2009, 24, 485–492.
- 12 H.-J. Bai and Z.-M. Zhang, Mater. Lett., 2009, 63, 764-766.
- 13 S. Stürzenbaum, M. Höckner, A. Panneerselvam, J. Levitt, J. Bouillard, S. Taniguchi, L. Dailey, R. A. Khanbeigi, E. Rosca and M. Thanou, *Nat. Nanotechnol.*, 2013, 8, 57–60.
- 14 L. Berti and G. A. Burley, Nat. Nanotechnol., 2008, 3, 81-87.
- 15 L. Gao and N. Ma, ACS Nano, 2011, 6, 689-695.
- 16 J. M. Pérez-Donoso, J. P. Monrás, D. Bravo, A. Aguirre, A. F. Quest, I. O. Osorio-Román, R. F. Aroca, T. G. Chasteen and C. C. Vásquez, *PLoS One*, 2012, 7, e30741.
- 17 F. Liu, S. H. Kang, Y.-I. Lee, Y. Choa, A. Mulchandani, N. V. Myung and W. Chen, *Appl. Phys. Lett.*, 2010, 97, 123703.
- 18 F. Baneyx and D. T. Schwartz, Curr. Opin. Biotechnol., 2007, 18, 312–317.
- R. Dunleavy, L. Lu, C. J. Kiely, S. McIntosh and B. W. Berger, *Proc. Natl. Acad. Sci. U. S. A.*, 2016, **113**, 5275–5280.
- 20 L. C. Spangler, L. Lu, C. J. Kiely, B. W. Berger and S. McIntosh, *J. Mater. Chem. A*, 2016, 4, 6107–6115.
- 21 L. C. Spangler, R. Chu, L. Lu, C. J. Kiely, B. W. Berger and S. McIntosh, *Nanoscale*, 2017, 9, 9340–9351.
- 22 Q. Li, X. Li, S. Wageh, A. A. Al-Ghamdi and J. Yu, *Adv. Energy Mater.*, 2015, 5, 1500010.
- 23 N. I. Kovtyukhova, P. J. Ollivier, B. R. Martin, T. E. Mallouk, S. A. Chizhik, E. V. Buzaneva and A. D. Gorchinskiy, *Chem. Mater.*, 1999, 11, 771–778.
- 24 S. Stankovich, D. A. Dikin, R. D. Piner, K. A. Kohlhaas, A. Kleinhammes, Y. Jia, Y. Wu, S. B. T. Nguyen and R. S. Ruof, *Carbon*, 2007, 45, 1558–1565.

Paper

- 25 G. Xie, K. Zhang, B. Guo, Q. Liu, L. Fang and J. R. Gong, *Adv. Mater.*, 2013, 25, 3820–3839.
- 26 Q. Li, B. Guo, J. Yu, J. Ran, B. Zhang, H. Yan and J. R. Gong, *J. Am. Chem. Soc.*, 2011, 133, 10878–10884.
- 27 H. Shin, K. K. Kim, A. Benayad, S. Yoon, H. K. Park, I. Jung, M. H. Jin, H. Jeong, J. M. Kim and J. Choi, *Adv. Funct. Mater.*, 2009, 19, 1987–1992.
- 28 Y. Xu and M. A. Schoonen, Am. Mineral., 2000, 85, 543-556.
- 29 C. Shan, H. Yang, D. Han, Q. Zhang, A. Ivaska and L. Niu, *Langmuir*, 2009, **25**, 12030–12033.
- 30 S.-H. Hu, Y.-W. Chen, W.-T. Hung, I.-W. Chen and S.-Y. Chen, *Adv. Mater.*, 2012, 24, 1748–1754.
- 31 V. Hlady and J. Buijs, Curr. Opin. Biotechnol., 1996, 7, 72.
- 32 D. C. Dittmer, in *Encyclopedia of Reagents for Organic Synthesis*, 2001.
- 33 Z. Yang, L. Lu, V. F. Berard, Q. He, C. J. Kiely, B. W. Berger and S. McIntosh, *Green Chem.*, 2015, 17, 3775–3782.
- 34 L. C. Spangler, J. P. Cline, C. J. Kiely and S. McIntosh, *Nanoscale*, 2018, **10**, 20785–20795.
- 35 A. Sadeghnejad, L. Lu, C. J. Kiely, B. W. Berger and S. McIntosh, RSC Adv., 2017, 7, 38490–38497.
- 36 D. Luo, G. Zhang, J. Liu and X. Sun, J. Phys. Chem. C, 2011, 115, 11327–11335.
- 37 B. Clark, T. Frost and M. Russell, *UV Spectroscopy: Techniques, instrumentation and data handling*, Springer Science & Business Media, 1993, vol. 4.
- 38 D. Chen, L. Li and L. Guo, *Nanotechnology*, 2011, 22, 325601.
- 39 C. Zhang, W. Lv, W. Zhang, X. Zheng, M.-B. Wu, W. Wei, Y. Tao, Z. Li and Q.-H. Yang, Adv. Energy Mater., 2014, 4, 1301565.
- 40 K. Krishnamoorthy, M. Veerapandian, K. Yun and S.-J. Kim, *Carbon*, 2013, 53, 38.
- 41 H.-L. Guo, X.-F. Wang, Q.-Y. Qian, F.-B. Wang and X.-H. Xia, *ACS Nano*, 2009, 3, 2653–2659.
- 42 M. Rozenberg and G. Shoham, *Biophys. Chem.*, 2007, 125, 166.

- 43 F. Tuinstra and J. L. Koenig, *J. Chem. Phys.*, 1970, **53**, 1126–1130
- 44 M. J. Matthews, M. A. Pimenta, G. Dresselhaus, M. S. Dresselhaus and M. Endo, *Phys. Rev. B: Condens. Matter Mater. Phys.*, 1999, 59, R6585–R6588.
- 45 Q. Sun, R. Collins, S. Huang, L. Holmberg-Schiavone, G. S. Anand, C. H. Tan, S. van-den-Berg, L. W. Deng, P. K. Moore, T. Karlberg and J. Sivaraman, *J. Biol. Chem.*, 2009, 284, 3076–3085.
- 46 A. E. Martell and R. M. Smith, *Critical stability constants*, Springer, 1974, vol. 1.
- 47 J. Wang, E. C. Salihi and L. Åiller, *Mater. Sci. Eng.*, C, 2017, 72, 1.
- 48 S. Thakur and N. Karak, Carbon, 2012, 50, 5331.
- 49 E. C. Salas, Z. Sun, A. Lüttge and J. M. Tour, ACS Nano, 2010, 4, 4852–4856.
- 50 G. Wang, F. Qian, C. W. Saltikov, Y. Jiao and Y. Li, *Nano Res.*, 2011, 4, 563–570.
- 51 S. Gurunathan, J. W. Han, V. Eppakayala and J.-H. Kim, *Colloids Surf.*, *B*, 2013, **102**, 772.
- 52 S. Rupp, in *Fundamentals and Application of New Bioproduction Systems*, ed. A.-P. Zeng, Springer Berlin Heidelberg, Berlin, Heidelberg, 2013, pp. 103–123.
- 53 W. W. Yu, L. Qu, W. Guo and X. Peng, *Chem. Mater.*, 2003, 15, 2854–2860.
- 54 O. Bunsho, Chem. Lett., 2008, 37, 216-229.
- 55 K. Ojha, T. Debnath, P. Maity, M. Makkar, S. Nejati, K. V. Ramanujachary, P. K. Chowdhury, H. N. Ghosh and A. K. Ganguli, J. Phys. Chem. C, 2017, 121, 6581–6588.
- 56 S. Mondal, S. Sudhu, S. Bhattacharya and S. K. Saha, J. Phys. Chem. C, 2015, 119, 27749–27758.
- 57 N. Zhang, Y. Zhang, X. Pan, X. Fu, S. Liu and Y.-J. Xu, J. Phys. Chem. C, 2011, 115, 23501–23511.
- 58 J. Zhang, J. Yu, M. Jaroniec and J. R. Gong, *Nano Lett.*, 2012, **12**, 4584–4589.
- 59 L. Jia, D.-H. Wang, Y.-X. Huang, A.-W. Xu and H.-Q. Yu, *J. Phys. Chem. C*, 2011, **115**, 11466–11473.